AIP | Journal of Applied Physics

Layering and temperature-dependent magnetization and anisotropy of naturally produced Ni/NiO multilayers

S. D. Pappas, V. Kapaklis, A. Delimitis, P. E. Jönsson, E. Th. Papaioannou, P. Poulopoulos, P. Fumagalli, D. Trachylis, M. J. Velgakis, and C. Politis

Citation: Journal of Applied Physics **112**, 053918 (2012); doi: 10.1063/1.4750026
View online: http://dx.doi.org/10.1063/1.4750026
View Table of Contents: http://scitation.aip.org/content/aip/journal/jap/112/5?ver=pdfcov
Published by the AIP Publishing

Layering and temperature-dependent magnetization and anisotropy of naturally produced Ni/NiO multilayers

S. D. Pappas,[1,a)] V. Kapaklis,[2] A. Delimitis,[3] P. E. Jönsson,[2] E. Th. Papaioannou,[2] P. Poulopoulos,[1,4,5] P. Fumagalli,[4] D. Trachylis,[1] M. J. Velgakis,[1] and C. Politis[1,6]
[1]*Laboratory of High-Tech Materials, School of Engineering, University of Patras, 26504 Patras, Greece*
[2]*Department of Physics and Astronomy, Uppsala University, Box 516, SE-751 20 Uppsala, Sweden*
[3]*Chemical Process Engineering Research Institute (CPERI), Centre for Research & Technology Hellas (CERTH), 57001 Thermi, Thessaloniki, Greece*
[4]*Institut für Experimentalphysik, Freie Universität Berlin, Arnimallee 14, D-14195 Berlin-Dahlem, Germany*
[5]*Materials Science Department, University of Patras, 26504 Patras, Greece*
[6]*Department of Materials Science and Engineering, University of Texas at Arlington, Arlington, Texas 76019, USA*

(Received 29 May 2012; accepted 9 August 2012; published online 11 September 2012)

Ni/NiO multilayers were grown by magnetron sputtering at room temperature, with the aid of the natural oxidation procedure. That is, at the end of the deposition of each single Ni layer, air is let to flow into the vacuum chamber through a leak valve. Then, a very thin NiO layer (~1.2 nm) is formed. Simulated x-ray reflectivity patterns reveal that layering is excellent for individual Ni-layer thickness larger than 2.5 nm, which is attributed to the intercalation of amorphous NiO between the polycrystalline Ni layers. The magnetization of the films, measured at temperatures 5–300 K, has almost bulk-like value, whereas the films exhibit a trend to perpendicular magnetic anisotropy (PMA) with an unusual significant positive interface anisotropy contribution, which presents a weak temperature dependence. The power-law behavior of the multilayers indicates a non-negligible contribution of higher order anisotropies in the uniaxial anisotropy. Bloch-law fittings for the temperature dependence of the magnetization in the spin-wave regime show that the magnetization in the multilayers decreases faster as a function of temperature than the one of bulk Ni. Finally, when the individual Ni-layer thickness decreases below 2 nm, the multilayer stacking vanishes, resulting in a dramatic decrease of the interface magnetic anisotropy and consequently in a decrease of the perpendicular magnetic anisotropy.
[http://dx.doi.org/10.1063/1.4750026]

I. INTRODUCTION

Magnetic ultrathin films and multilayers have attracted considerable interest the last decades. The decrease of the magnetic layer thickness and the introduction of interfaces result in new phenomena, which have changed the route of fundamental Physics and are exploited in many applications.[1–7] Temperature-dependent magnetization and anisotropy for thin magnetic layers provide insight in the understanding of ferromagnetism and test the validity of the theory.[8] Changing the magnetic anisotropy of a magnetic thin film from the in-plane to out-of-plane direction is a technological challenge and in the case of magnetic multilayers, this can be done by periodically interrupting the magnetic material forming magnetic/non magnetic interfaces. As the individual magnetic layers become thinner, the contribution of a positive interface anisotropy K_S may dominate that of the volume anisotropy resulting in the rotation of the easy magnetization direction from in-plane to out-of plane.[9] The sign of interface anisotropy, however, is a characteristic of the interface formed by the magnetic material and the barrier layer. In the case of Co and Fe, the interface anisotropies are usually positive, whereas for the Ni-based multilayers are close to zero or negative.[2,3,9] For that reason, perpendicular magnetic anisotropy (PMA) in Ni films is attributed mainly to magnetoelastic anisotropy[3,8] and not to the interface anisotropy.

In this work, we focus on the layering quality and the temperature-dependent magnetic properties of Ni/NiO multilayers produced by natural oxidation.[10,11] Natural oxidation is described as the oxidation at the top of a freshly deposited thin film by letting air or oxygen to flow in the growth chamber. CoFe/oxide multilayers prepared by this method (oxygen flow) exhibited amorphous oxide layers 2–3 nm thick and showed excellent properties such as high magnetic moment, very small coercivity, and high resistivity for high frequency applications of magnetic recording heads.[12] Nickel is an excellent candidate, compared to CoFe, for the formation of multilayers with protective NiO layers with high stability upon exposure to oxygen or air. This feature of Ni is explained by the favorable value of 1.52 for its Pilling-Bedworth (P-B) ratio[13]

$$\text{P-B ratio} = A_O\rho_M/A_M\rho_O. \quad (1)$$

Here, A_O is the molecular weight of the oxide and ρ_O its density, while A_M and ρ_M are the corresponding values for the metal. P-B ratio values in the range of 1–2 favor the formation of protective oxide layers. For values <1, the oxide layer is usually porous and, therefore, it cannot be protective

a)Author to whom correspondence should be addressed. Electronic mail: spappas@upatras.gr. Tel.: +30-2610-997884. Fax: +30-2610-997255.

as the oxide does not fully cover the metal surface. For values >2–3, the oxide coating may crack, leaving this way unprotected metallic surfaces. The P-B ratio value for Ni is 1.52 and, therefore, a NiO protective oxide layer is easily formed.

In this study, the layering quality of Ni/NiO multilayers with Ni thickness in the range 1–6 nm is evaluated. For Ni thickness larger than 2.5 nm, the multilayers consist of smooth continuous layers with small roughness, as x-ray reflectivity (XRR) and computer simulation reveal. Both, high resolution transmission electron microscopy (HRTEM) and magnetic characterization reveal the formation of discontinuous Ni layers for a Ni thickness below about 2 nm. That is, there are Ni crystallites but they do not form continuous layers anymore. This structural transformation results in a decrease of both the magnetic moment and magnetic anisotropy. All multilayers demonstrate considerable positive interface anisotropy, which is unexpected for Ni-based multilayers. The value of the interface anisotropy constant K_s is about $+0.135$ erg/cm^2 ($+0.135$ mJ/m^2) at 5 K; whereas at room temperature, it decreases to $+0.11$ erg/cm^2 ($+0.11$ mJ/m^2). These values are coming from statistics over 5–6 samples, so they are accurate within an error bar less than 10%. The magnetization hysteresis loops show features characteristic for the formation of up and down magnetic domains at low temperatures indicating that the local magnetizations stay perpendicular to the film plane at remanence. The temperature dependence of the magnetization and anisotropy are discussed within the framework of mean field theories.

II. EXPERIMENTAL DETAILS

Ni/NiO multilayers were grown on the native oxide of Si (100) wafers and on glass by means of a radio frequency magnetron (r.f.) sputtering head in a vacuum chamber with base pressure of 5×10^{-6} Pa. First, Ni was grown at constant r.f. power of 30 W and Ar pressure at 0.3 Pa. At the end of the deposition of each Ni layer, air was introduced in the chamber via a leak valve at 0.2 Pa partial pressure for 1 min. By this method, a thin saturated layer of NiO with thickness of ~1.2 nm is formed on the top of the Ni layer. The air flow was then interrupted and followed by a pause for ~3 min before depositing the next layer, thus allowing the oxygen pressure to drop to its background level. The procedure is repeated *N* times, where *N* is the desired number of the multilayer periods. A series of 9 Ni/NiO multilayers with 6–21 repetitions and a total thickness in the 50 nm range were fabricated by the aforementioned procedure. The individual Ni-layer thickness varied between 1–6 nm. No traces of nitrogen were found.[10] The result is the same (amorphous oxide formation) as if one uses oxygen.[12]

Structural characterization of the Ni/NiO multilayers and the layering quality was performed with the aid of the XRR technique and via HRTEM experiments. The XRR measurements were carried out using a Phillips XPert PW3020 diffractometer in Bragg-Brentano geometry, with CuKα radiation ($\lambda = 1.5418$ Å). Samples grown on Si or glass were shown to be almost identical. Selected films suitable for transmission electron microscopy (TEM-HRTEM) experiments were prepared by mechanical polishing followed by gentle Ar ion milling. The TEM experiments were carried out in a JEOL 2011 electron microscope, operating at 200 kV with a resolution of 0.23 nm. The instrument is also fitted with an energy-dispersive x-ray spectroscopy (EDS) detector for the elemental analysis of the samples. Qualitative and semi-quantitative analysis of EDS data were accomplished using the INCA microanalysis suite software package. First, results showed that Ni is mainly {111} textured and the NiO layers are amorphous.[10]

Superconducting quantum interference device (SQUID) magnetometry measurements of the Ni/NiO multilayers were performed at temperatures T = 5, 100, 150, 200, and 300 K and under maximum field of 5 T. An MPMS XL-7 magnetometer was used for the measuring of the magnetic loop of each sample in the perpendicular and in the plane field direction. The effective anisotropy K_{eff} of each sample was determined by calculating the area which is formed between the in-plane magnetic loop of the material and the out-of-plane loop. In the case of hysteresis, averaging of the loops was performed and K_{eff} was determined by the anhysteretic curves. K_{eff} is positive (negative) for out-of-plane (in-plane) magnetized films. The contribution of the diamagnetic background, coming from the Si(001) wafer in the case of the

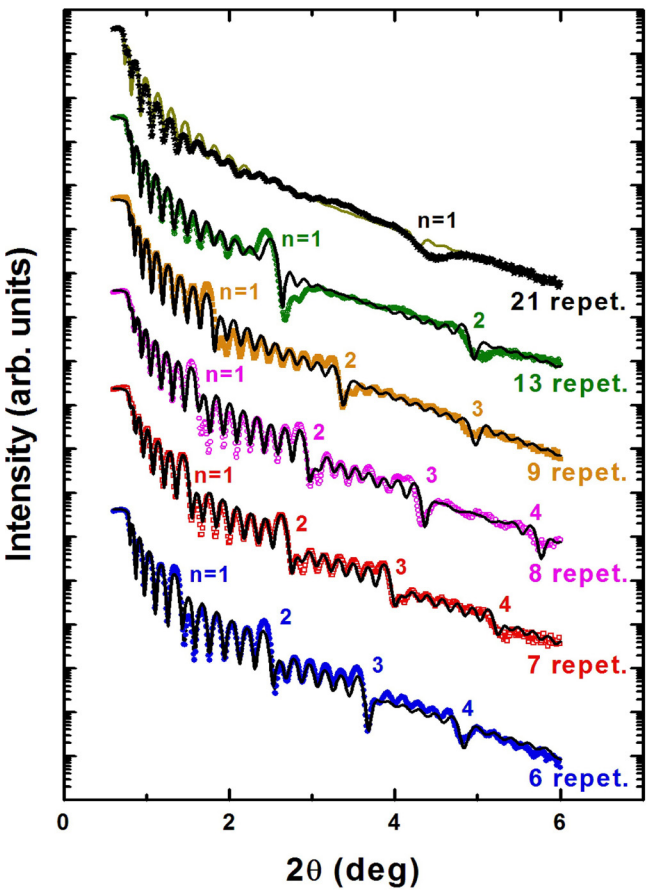

FIG. 1. XRR spectra of the Ni/NiO multilayers. The symbols correspond to the experimental data, whereas the solid lines are the fittings of the experimental data obtained with the help of the GenX code. The spectra have been vertically shifted for clarity. The results from the fittings are summarized in Table I.

TABLE I. Data for the series of Ni/NiO multilayers whose XRR patterns are included in Fig. 1. The values were obtained via the use of GenX code for simulation. The simulated thickness of the layers, as well as the simulated r.m.s. roughness are expressed in nm. The unrealistic values of roughness as the thickness decreases is related to the transition from continuous to discontinuous Ni layers as we will show in Sec. IV.

No. of repetitions	Ni thickness (nm)	NiO thickness (nm)	RMS Ni roughness (nm)	RMS NiO roughness (nm)
6	6.057	1.357	0.365	0.325
7	5.669	1.179	0.548	0.650
8	4.985	1.284	0.652	0.357
9	4.243	1.137	0.536	0.376
13	2.49	1.160	2	1.00
21	0.963	1.146	4.00	0.335

in-plane measurements, as well as of the paramagnetic background, coming from the sample mounting in the case of the out-of-plane measurements, were removed by subtracting the slopes from the raw SQUID data.

III. XRR PATTERNS AND LAYERING

With the help of the XRR patterns of the multilayers, shown in Fig. 1, information such as the bilayer thickness, layer roughness, as well as the quality of the layering can be extracted. From the relative positions of the multilayer peaks labelled with a natural number "*n*," the thickness of the multilayer period[14] can be estimated, whereas from the Kiessig fringes which are located between the multilayer peaks, the total thickness of the film can be extracted.[15] In our case, the XRR patterns were simulated with the help of the GenX code[16] in order to provide complementary information such as film roughness. The results from the fittings of selected Ni/NiO multilayers are all summarized in Table I, which readily show that the thickness of the naturally produced NiO (t_{NiO}) has an average value of about 1.17 nm and the deviation of the simulated t_{NiO} is within the calculated experimental error range in each case. The RMS roughness presented in Table I is the total roughness of the interfaces (σ_{tot}), which holds $\sigma_{tot}^2 \sim \sigma_r^2 + \sigma_i^2$.[16,17] σ_r is the roughness of the interface, which is introduced in the model as a sinusoidal modulation of the layer thickness on the top of each layer or interface, and σ_i is the interdiffusion. σ_{tot} monotonically increases with the number of repetitions. On the contrary, the σ_{tot} of the NiO layer is lower than that of Ni layer in all cases, which indicates a healing of the Ni layer roughness with oxidization. This roughness smoothing, caused by the amorphous layers, in crystalline/amorphous multilayers has been reported in earlier literature.[18] The XRR patterns have been simulated with the help of a single roughness value, which is an average roughness for all the NiO-Ni and Ni-NiO interfaces. For this reason, in the case of the multilayers with a large number of bilayer peaks, the spectra cannot be fitted perfectly[17] due to the possible accumulative roughness.[19]

IV. TEMPERATURE-DEPENDENT MAGNETIC PROPERTIES

Figure 2 shows the magnetization hysteresis loops at 5 K with the external field applied perpendicular (circles) and parallel (squares) to the film plane for 4 multilayers with $t_{Ni} = 6.1$ nm (a), 2.5 nm (b), 2.1 nm (c), and 1 nm (d). The symbol t_{Ni} stands for the thickness of Ni after the oxidation, i.e., it is the individual Ni layer thickness in the multilayer. The magnetization normalized per Ni volume is bulk-like for thick films and decreases proportionally with the

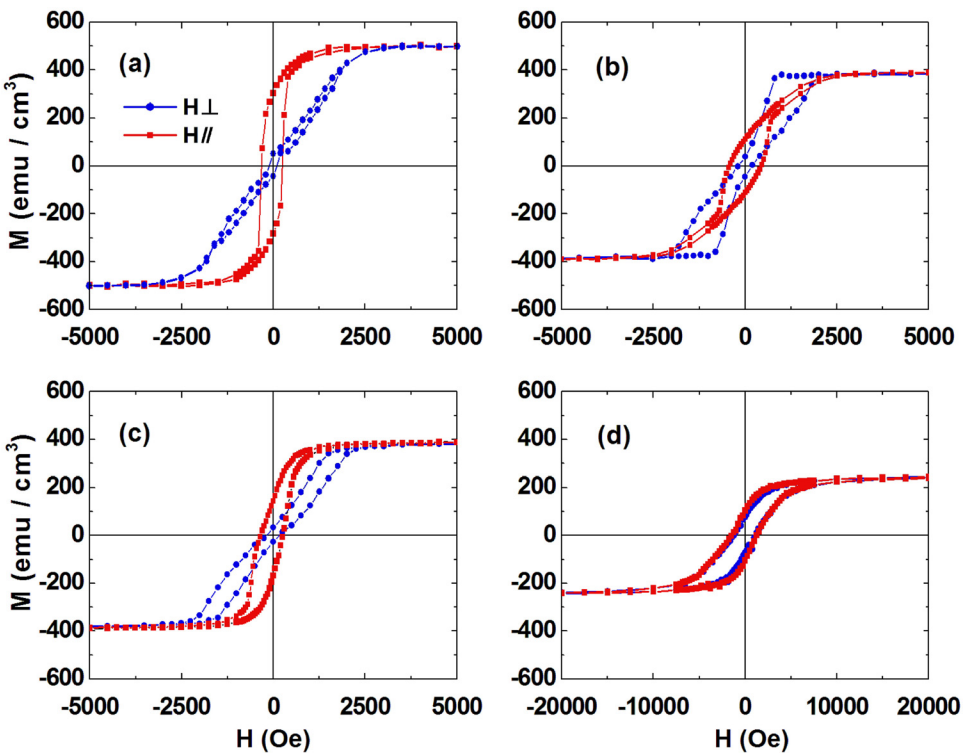

FIG. 2. Magnetization hysteresis loops recorded by SQUID at 5 K with the external field applied perpendicular (circles) and parallel (squares) to the film plane for 4 multilayers with $t_{Ni} = 6.1$ nm and 6 repetitions (a), 2.5 nm and 13 repetitions (b), 2.1 nm and 15 repetitions (c), and 1 nm and 21 repetitions (d).

individual Ni-layer thickness t_{Ni}. Linear regression in an Mt_{Ni} over t_{Ni} plot revealed that about 0.3 nm of Ni at each interface does not contribute to the magnetic response.[11] Furthermore, one may see that perpendicular magnetic anisotropy develops as the individual layer Ni-film thickness decreases from 6.1 nm down to 2.5 nm. The out-of-plane hysteresis loop for the sample with $t_{Ni} = 2.5$ nm is characteristic for a sample with up and down magnetic domains.[20] Similar in- and out-of-plane hysteresis loops were previously reported for a Ni/NiO multilayer with thick Ni layers, although grown at high Ar pressure, together with a magnetic force microscopy image showing up and down stripe magnetic domains.[10] The magnetic domains with up and down net magnetization are spontaneously formed in order to reduce the magnetostatic energy. Figure 2(c) reveals that further decrease of t_{Ni} to 2.1 nm degrades perpendicular magnetic anisotropy. Finally, at $t_{Ni} = 1$ nm, the in- and out-of-plane hysteresis loops become identical and the coercivity increases to 1.2 kOe, i.e., by one order of magnitude as compared to all other Ni/NiO multilayers. This interesting magnetic behavior of Ni/NiO multilayers will be explained in Sec. V with the aid of HRTEM.

In Fig. 3, we plot the temperature-dependent magnetization hysteresis loops for the sample with $t_{Ni} = 2.5$ nm, which is the one with the strongest tendency for perpendicular magnetic anisotropy. As aforementioned, at 5 K, Fig. 3(a), the loop with the external field applied normal to the film plane indicates the presence of up and down magnetic domains. However, the system evolves gradually as temperature increases to a magnetic film with parallel magnetization at room temperature, and hence a spin reorientation transition from out-of-plane to in-plane magnetization occurs similar to the one reported for ultrathin Fe films.[21,22] The temperature-driven spin-reorientation transition is an entropy effect[23] and can be explained by the fact that the uniaxial anisotropy decreases faster with temperature than the shape anisotropy, since the first is scaling as M^{Γ} where $\Gamma > 3$, as shown below, and the latter is scaling as M^2.

In Fig. 4, the normalized magnetization $M_N = M(T)/M(T = 5\,K)$ is shown for a series of Ni/NiO multilayers with individual Ni-layer thickness t_{Ni}, as indicated. For comparison, values for bulk Ni are used, obtained from Ref. 24. One may notice that for $t_{Ni} > 4$ nm, the temperature dependence of M_N is almost identical. This reflects the fact that the Curie temperature T_C of the individual Ni(111) layers, which are thicker than about 20 atomic layers, is bulk like, in agreement with Ref. 3. The slight reduction of the room temperature magnetization with respect to the bulk Ni could be attributed to a capping layer effect.[25] Considering that below about 30% of T_C, we are in the spin-wave regime, one may attempt a Bloch law fitting of $M_N = 1 - AT^{3/2}$ (Ref. 24). The constant A for bulk Ni has the experimental value of 0.75×10^{-5} $K^{-3/2}$ (Ref. 26). Fitting of our data for the film with the larger t_{Ni} provides a value $A = 1.38 \times 10^{-5}$ $K^{-3/2}$. The fast decrease of M_N for the films with the thinner Ni layers reflects the decrease of the T_C due to finite-size effects as well as an intense activity of spin waves towards the two dimensional limit (Mermin-Wagner theorem) see, e.g., Ref. 3. For the Ni/NiO with $t_{Ni} = 2.5$ nm, $A = 3.29 \times 10^{-5}$ $K^{-3/2}$. The fitting was done only up to 150 K due to decrease of T_C for this sample.[3] Similar influence of the magnetic layer thickness to the numerical values of the constant A has been also observed in Fe/V and Pd/Ni multilayers.[27–29]

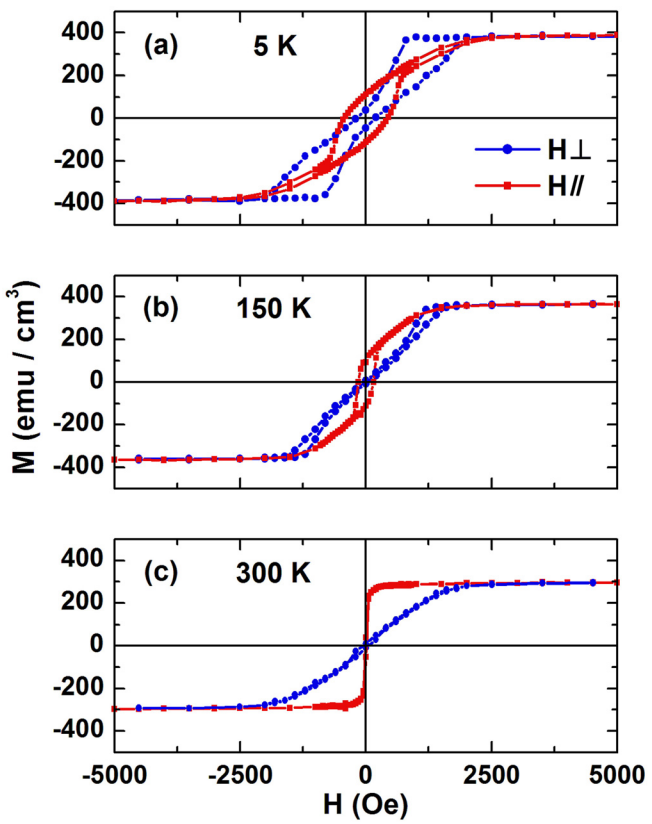

FIG. 3. Temperature-dependent magnetization hysteresis loops with the external filed applied perpendicular (circles) and parallel (squares) to the film plane for a Ni/NiO multilayer with $t_{Ni} = 2.5$ nm. The number of repetitions is 13.

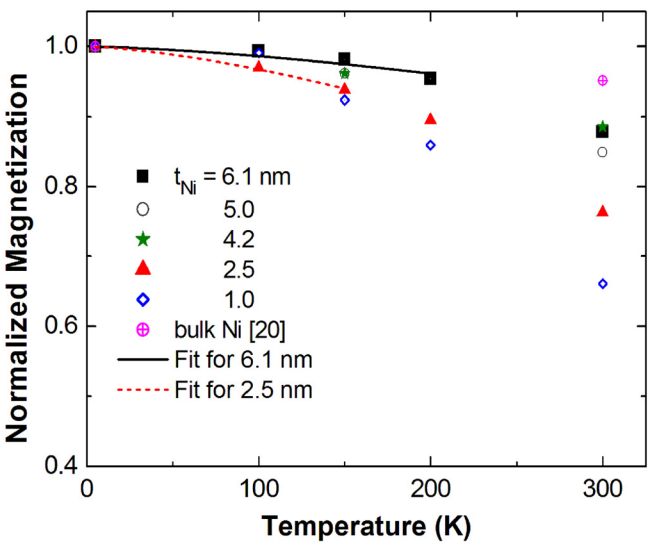

FIG. 4. Temperature-dependent normalized magnetizations (symbols) for a series of Ni/NiO multilayers as indicated. The lines are the results of Bloch-law fits in the spin-wave regime. For comparison, values for bulk Ni have been introduced from Ref. 20. The number of repetitions from the largest to smallest t_{Ni} is: 6, 8, 9, 13, and 21, respectively.

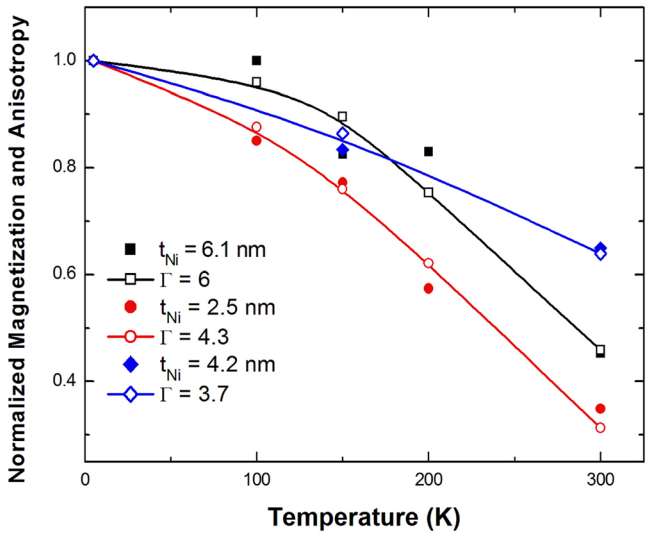

FIG. 5. Temperature-dependent normalized uniaxial anisotropies (closed symbols) and normalized magnetizations to the Γ power (open symbols) for representative Ni/NiO multilayers as indicated. The Γ values were determined by the coincidence of the M_N^{Γ} to the anisotropy data. The number of repetitions is 6 for $t_{Ni} = 6.1$ nm, 13 for $t_{Ni} = 2.5$ nm, and 9 for $t_{Ni} = 4.2$ nm.

Figure 5(a) depicts (closed symbols) the temperature dependence of the normalized uniaxial magnetic anisotropy $K_{uN} = K_u(T)/K_u(T = 5\,K)$ of representative multilayers. K_u was derived by K_{eff} after adding the magnetostatic anisotropy $2\pi M^2$.[2] Positive K_u values favor perpendicular magnetic anisotropy. In the same figure, data for the normalized magnetization to the Γ power $[M(T)/M(T = 5\,K)]^{\Gamma}$ have been introduced (open symbols—line). The Γ values were determined by making the temperature dependencies equal. They range between 3.7 and 6 for all samples. Following the thermodynamic local anisotropy model by Callen and Callen,[30] the normalized uniaxial magnetic anisotropy coefficients should vary as a function of the normalized magnetization to the $\Gamma = i(i+1)/2$ power

$$k_{ui}(T)/k_{ui}(T = 0\,K) \propto [M(T)/M(T = 0\,K)]^{\Gamma}, \qquad (2)$$

where i represents the order of the spherical anisotropy coefficients and k_{ui} are the different coefficients. The connection of the K_{ui} coefficients, which are used in the case where the analysis of the anisotropic part of the free energy is performed in terms of the direct cosines expansion, with the k_{ui} spherical anisotropy coefficients is presented in more detail in Refs. 8 and 32. Within the analysis of our experimental data, not only second order anisotropy coefficients, but also fourth and higher order coefficients may contribute in the uniaxial anisotropy coefficient K_u. Consequently, only for vanishing fourth and higher order coefficients, an exponent $\Gamma = 3$ is expected for the relationship $Ku(T)/Ku(T = 0\,K) = [M(T)/M(T = 0\,K)]^{\Gamma}$. Up to now, few works provide Γ values close to 3 for Fe films with measured negligible higher order anisotropies[31–33] and a Pd_4-Ni_2 multilayer.[25] On the other hand, a Γ value as large as 6.5 has been reported for 6 nm of Fe grown on W(110).[34] Following the argumentation of Refs. 8 and 30, the Γ values of our films result from non-vanishing higher order anisotropies with different strength. The less significant the value of the higher order anisotropies is, the closer the value of Γ to 3 becomes.

In Fig. 6, the $K_{eff} \cdot t_{Ni}$ over t_{Ni} analysis[2,3] of the multilayers is performed at the selected temperatures T = 5, 150, and 300 K. It should hold

$$K_{eff} \cdot t_{Ni} = K_v \cdot t_{Ni} + 2 \cdot K_s, \qquad (3)$$

where K_v is the volume anisotropy constant (K_v includes the magnetocrystalline anisotropy constant, the magnetoelastic anisotropy, and the magnetostatic or shape anisotropy) and K_s is the interface anisotropy constant due to the broken symmetry at the interfaces. By applying this analysis to our experimental data points, we can determine the K_v value from the slope of the line, as well as the K_s value from its intercept with the perpendicular axis. In the case of T = 5 K and T = 150 K, the experimental data points were obtained only from SQUID measurements, whereas in the case of T = 300 K, the experimental data points were obtained by the combination of SQUID and magneto-optical Kerr effect (MOKE) measurements. For the Ni/NiO multilayers at 5 K, it is deduced $K_v = -0.92 \times 10^6$ erg/cm^3 (-0.92×10^5 J/m^3) and $K_s = +0.135$ erg/cm^2 ($+0.135$ mJ/m^2). At T = 150 K, $K_v = -1.04 \times 10^6$ erg/cm^3 (-1.04×10^5 J/m^3) and $K_s = +0.13$ erg/cm^2 ($+0.13$ mJ/m^2) and at T = 300 K, $K_v = -1.1 \times 10^6$ erg/cm^3 (-1.1×10^5 J/m^3) and $K_s = +0.11$ erg/cm^2 ($+0.11$ mJ/m^2). The experimental accuracy is ±10%. The results of the linear regression show a positive value of interface anisotropy with weak temperature dependence. The positive value suggests tendency for perpendicular magnetic anisotropy. The effect is surprising and was initially discussed in Ref. 10. A similar tendency of thin Ni films, grown on the Cu-CuO stripe phase, after post-growth oxygen exposure has been recently reported.[35,36] Finally, the relatively weak temperature dependence of K_s in our multilayers is in agreement with previous reports for the

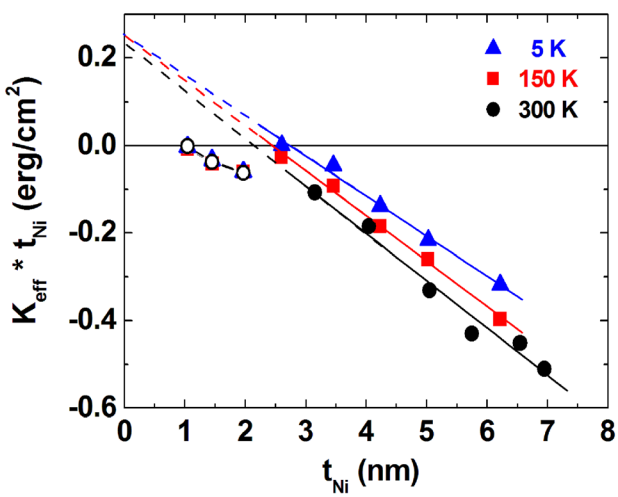

FIG. 6. Kt over t plot of the Ni/NiO multilayers at T = 5, 150, and 300 K. The lines correspond to the linear fit of the experimental data points (closed symbols) at each temperature. The slope of the curves and the intercept of them with the y axis allow us to calculate the K_v and K_s values, respectively. The error bar of K_v and K_s values is ~10%. The open symbols represent experimental data points for the 3 films with thin Ni layers, which fail to the fits.

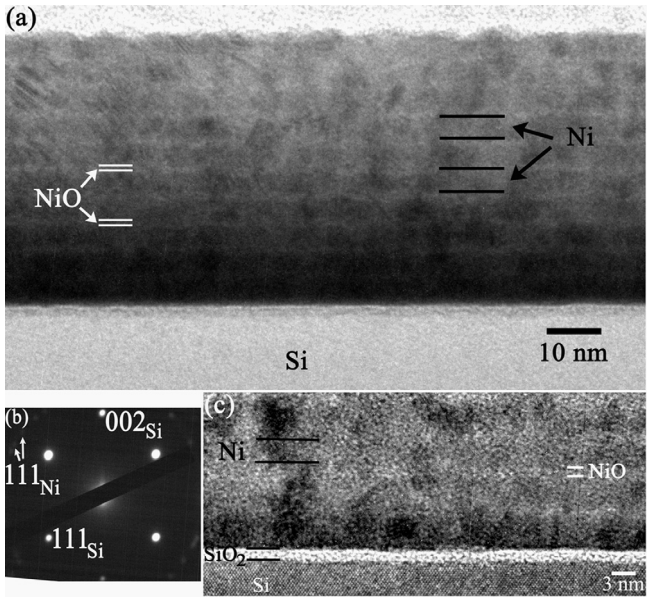

FIG. 7. (a) TEM image showing the morphology of a Ni/NiO well-ordered multilayer having 10 repetitions and nominal thickness $t_{Ni} = 3.5$ nm. (b) SAD pattern obtained from the interfacial area of Si/SiO_2/multilayer, revealing the nanocrystalline structure of the Ni layers. Diffraction spots attributed to Si are also denoted in the image, corresponding to its [110] zone axis. (c) Higher magnification image of an area close to the interface between Ni/NiO and the Si substrate, depicting the nanograin architecture of the Ni layers and the amorphous NiO spacers.

temperature dependence of interface magnetic anisotropy in Co/Pt magnetic multilayers.[37]

V. CORRELATION BETWEEN MAGNETISM AND STRUCTURE

One may see that K_s becomes more important in Eq. (3) as t_{Ni} decreases down to 2.5 nm due to the existence of a larger number of interfaces for a predetermined film thickness. However, application of Eq. (3) to the multilayer with the thickest Ni layer at 5 K reveals that K_s is responsible for less than half of the value of the uniaxial anisotropy K_u. Magnetocrystalline anisotropy of bulk Ni is very small[24] and consequently, the only other contribution should be magnetoelastic anisotropy. Therefore, evidence is required for the potential existence of residual anisotropic strain in the Ni layers.[38] Furthermore, the deviation from linear behavior the $K_{eff} \cdot t_{Ni}$ over t_{Ni} plot shows for $t_{Ni} < 2.5$ nm is indeed intriguing.

In order to correlate the aforementioned points with the structure of the films, electron microscopy methods were used to study selected Ni/NiO multilayers. In Fig. 7(a), the TEM image illustrates the growth of a multilayer with continuous layers and discrete and sharp interfaces with $t_{Ni} > 2.5$ nm range of thickness. The multilayer is grown on top of the single crystalline Si(100) substrate, where the development of an intrinsically grown SiO_2 layer is also observed. The Ni layers comprise of small nanograins as proved by the multiple Ni spots in the selected area diffraction (SAD) pattern of Fig. 7(b) whose size is limited by t_{Ni}, i.e., their growth stops at the entirely amorphous NiO layers. The nanograin growth is also obvious at the higher magnification image in Fig. 7(c), where the interfacial quality of the Ni/NiO and NiO/Ni interfaces is also presented in more detail.

The distribution of residual strain inside the Ni nanograins was calculated by the geometric phase analysis (GPA) method.[39] By means of "distribution," we imply how the residual strain is spread/dispersed across the Ni grains after the growth of the Ni/NiO multilayer was accomplished. The method uses the phase part of each of the complex Fourier components an HRTEM image is made up from in reverse space. GPA images are highly sensitive to slight differences between lattice fringe spacing in HRTEM images of nanoparticles, which can be an effect of residual strain or chemical variations inside them. The results from GPA for the Ni/NiO multilayer are outlined in Fig. 8. The phase images and the corresponding strain maps of Figs. 8(b) and 8(c), respectively, refer to the two circled Ni grains of the HRTEM image in Fig. 8(a) and were created using $\boldsymbol{g} = 111$ of Ni as the diffraction vector. They reveal a uniform strain distribution inside the Ni nanograins, where the maximum peak-to-peak difference is up to $(3 \pm 1)\%$ on average, as depicted in the strain profile acquired across a typical Ni grain, Fig. 8(d). Since the Ni grains have a {111} texture,[10] this strain should be anisotropic and may well stem from point lattice defects, interstitial atoms, and/or impurities inside the Ni matrix. Furthermore, areas where the strain differences are slightly

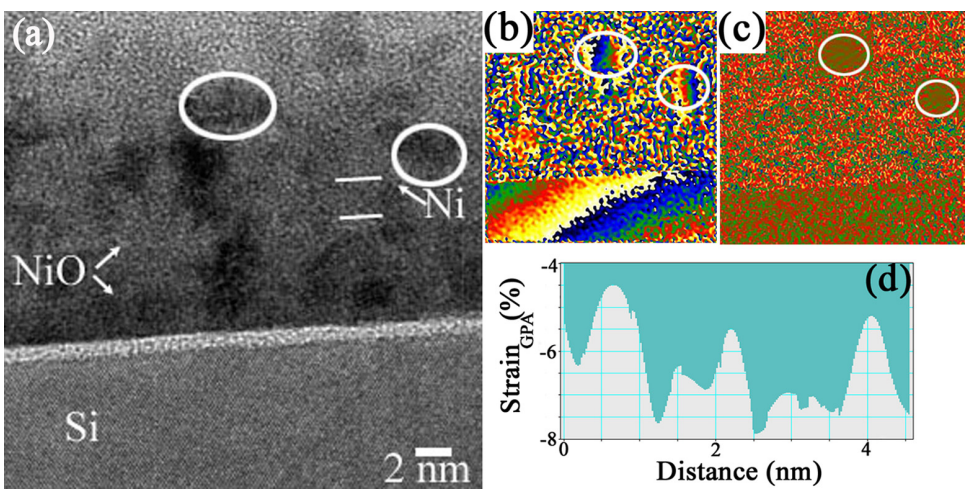

FIG. 8. Strain analysis results obtained by GPA in individual Ni grains of the multilayer with 10 repetitions and nominal thickness $t_{Ni} = 3.5$ nm (a) HRTEM image depicting the individual grain atomic structure, (b) phase image created using the 111 spatial frequencies of the two grains circled, (c) corresponding strain map calculated by the phase images. The strain profile across the top Ni grain is plotted in (d).

higher (~3.5%) could indicate the presence a very low O content inside them—in the form of Ni-O bonds—since the lattice strain [$Strain_{(NiO\text{-}Ni)}$] between well-formed crystalline NiO ($a = 0.4177$ nm) and metallic Ni ($a = 0.3524$ nm) is higher than 18%, according to the formula

$$Strain_{(NiO-Ni)} = (d_{111}{}^{NiO} - d_{111}{}^{Ni})/d_{111}{}^{Ni} = +18.58\%. \quad (4)$$

This is also in accordance with detailed measurements of the interplanar spacings in the Ni grains that were performed in typical HRTEM micrographs, where a mean value of 0.207 nm was estimated. This value corresponds to the spacing of the {111} crystal planes of bulk metallic Ni[10,24] and was found to be slightly higher (1.8%) than its theoretical one. The existence of anisotropic strain in the samples may well account for their magnetoelastic anisotropy.[37]

In Fig. 9(a), a cross section transmission electron microscopy (XTEM) image of the multilayer with the thinnest Ni layers, $t_{Ni} = 0.96$ nm, is shown. This reveals an almost homogeneous structure (discontinuous layers), than an ideal multilayered film. The TEM imaging experiments revealed that the Ni/NiO epilayer seems to grow in a compact mode of growth on top of Si, with no discrete layers of Ni or NiO formed. The total epilayer thickness is 46 nm, with an average roughness value of 2–3 nm. SAD experiments were performed in several areas in the sample and confirmed that the epilayer is generally amorphous, as shown in the pattern of Fig. 9(b), where only reflections from the Si substrate are evident. Only occasional nanocrystalline grains were detected by HRTEM observations, such as the one presented in Fig. 9(c). The grains have sizes up to 4 nm, they usually exhibit {111} type lattice fringes and do not have a specific shape or orientation with respect to the Si substrate. The chemical synthesis of this sample was also measured by EDS. The EDS results revealed that the Ni/O ratio is about 1.79, which is in good agreement with the XRR results, according to which $t_{Ni} = 0.96$ nm and $t_{NiO} = 1.16$ nm, and the Ni/O overall ratio is calculated to be 1.83. These results confirm that the interface between the Ni and NiO layers is not well defined, although the overall stoichiometry is preserved. The degraded quality of the interfaces between the Ni and NiO layers is also confirmed from the XRR results of the multilayer, where the bilayer peak is very broad and of low intensity. Furthermore, EDS revealed that the Ni/O ratio is even lower in the areas close to the free surface of the epilayer compared to these located in the middle of the film, as a result of the increase of the O content predominately. This indicates a migration of O atoms towards the epilayer free surface, which also enhances the amorphous morphology of the Ni/NiO film.

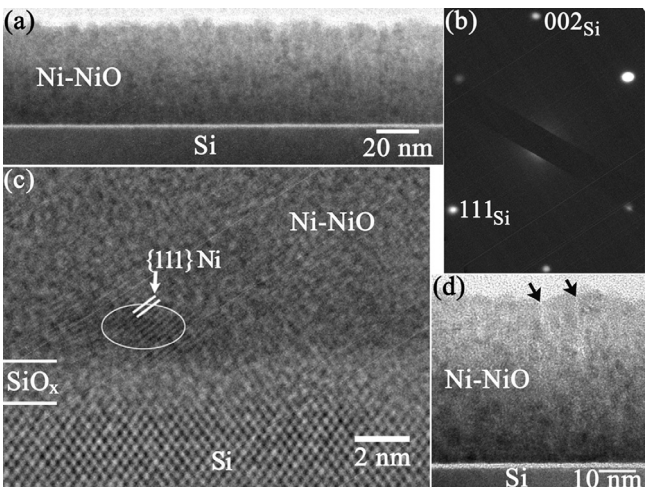

FIG. 9. (a) TEM image from a Ni/NiO multilayer with $t_{Ni} < 2.5$ nm illustrating an amorphous morphology throughout the whole epilayer. This is further confirmed by the SAD pattern in (b), obtained from the interface between Ni/NiO and the Si substrate where only spots corresponding to [110] projection of Si are included. (c) HRTEM image obtained from the Ni/NiO interfacial region, revealing the existence of only a few Ni nanograins embedded in the amorphous Ni/NiO matrix. The grains do not have a specific orientation with respect to the Si substrate. (d) Higher magnification TEM image illustrating the columnar island morphology of the Ni/NiO epilayer. Black arrows depict the boundaries between the distinct columns throughout the whole film.

TEM imaging experiments at higher magnifications were also performed for this sample, and a typical image is presented in Fig. 9(d). This shows more clearly that, at small thickness, the Ni film is not longer horizontally multilayered, but there are quite a few areas where it is divided [shown by white arrows in Fig. 9(d)] into small islands with a columnar morphology. Then, the magnetic/non magnetic interface area is reduced and consequently the contribution of the surface anisotropy K_s to the effective anisotropy constant K_{eff} will be decreased. This assumption is well fitted to our results, since the $K_{eff} \cdot t_{Ni}$ product posses a reduction, for the multilayers with thin Ni layers. Furthermore, the partial loss of crystallinity should also result in a decrease of the magnetoelastic anisotropy. The magnetic measurements however seem to exclude the formation of a homogeneous amorphous film. Such films or multilayers are expected to be magnetically soft, see, e.g., Ref. 40. However, Fig. 2(d) reveals that the film with the thinnest Ni layers is magnetically hard presenting the largest coercivity of all samples. The appearance of a large coercivity is an evidence of large magnetic anisotropy (magnetocrystalline + interface + magnetoelastic), which obviously is not the case for this sample and/or structurally and magnetically inhomogeneous magnetic materials.[24] Therefore, combination of HRTEM and SQUID measurements suggest that in the sample with the thinnest Ni layers, there is an inhomogeneous distribution of discontinuous Ni layers and a very high density of defects and localized strain, which result in partial amorphization of the magnetic Ni layers and increase of coercivity by one order of magnitude compared to the other samples.

VI. CONCLUSIONS

In this work, the layering of crystalline/amorphous Ni/NiO multilayers with individual Ni-layer thickness between 1-6 nm and constant NiO thickness ~1.2 nm has been investigated using a combination of x-ray reflectivity experiments and simulation and high resolution transmission electron microscopy. The layering is excellent for samples with $t_{Ni} > 2.5$ nm, but degrades below this thickness, and finally for $t_{Ni} = 1$ nm, the layers become discontinuous and

partially amorphous. These structural changes result in the decrease of the magnetic/non magnetic area, having a dramatic influence on the magnetic properties, such as the decrease of the surface anisotropy and the decrease of the effective anisotropy. Tendency for perpendicular magnetic anisotropy is exhibited and this is attributed to an unusual, for Ni-based multilayers, positive interface anisotropy, and the presence of a small anisotropic strain, which is more important for samples with large t_{Ni}. The temperature dependence of magnetization and anisotropy of the samples is measured and compared to theoretical models. The power-law behavior of the multilayers with continuous Ni layers indicates that there is a non-negligible contribution of higher order anisotropies in the uniaxial anisotropy. Furthermore, by attempting a Bloch law fitting of the temperature dependence of the magnetization in the spin-wave regime, it is shown that the magnetization of the multilayers decreases faster with decreasing t_{Ni}, showing more intense spin-wave effects in the thinner Ni layers.

ACKNOWLEDGMENTS

This work has been supported by the Research Committee of the University of Patras, Grant Karatheodori, No. C.905/2009. One of us (P.P.) would like to thank the Center for International Cooperation (C.I.C.) of the Freie Universität Berlin for partial financial support and the Institute for Experimental Physics, Freie Universität Berlin, for their generous hospitality. Also, P.E.J. acknowledges financial support from the Swedish Research Council (VR) and the Göran Gustafsson Foundation. And finally, we would like to thank the TSMEDE funds for partial financial support of this work.

[1]P. F. Carcia, A. D. Meinhaldt, and A. Suna, Appl. Phys. Lett. **47**, 178 (1985).
[2]W. J. M. de Jonge, P. J. H. Bloemen, and F. J. A. den Broeder, *Ultrathin Magnetic Structures I*, edited by J. A. C. Bland and B. Heinrich (Springer-Verlag, Berlin, 1994), pp. 65–90.
[3]P. Poulopoulos and K. Baberschke, J. Phys.: Condens. Matter **11**, 9495 (1999).
[4]F. Wilhelm, P. Poulopoulos, G. Ceballos, H. Wende, K. Baberschke, P. Srivastava, D. Benea, H. Ebert, M. Angelakeris, N. K. Flevaris, D. Niarchos, A. Rogalev, and N. B. Brookes, Phys. Rev. Lett. **85**, 413 (2000).
[5]F. Wilhelm, P. Poulopoulos, H. Wende, A. Scherz, K. Baberschke, M. Angelakeris, N. K. Flevaris, and A. Rogalev, Phys. Rev. Lett. **87**, 207202 (2001).
[6]C. A. F. Vaz, J. A. C. Bland, and G. Lauhoff, Rep. Prog. Phys. **71**, 056501 (2008).
[7]M. Bibes, J. E. Villegas, and A. Barthélémy, Adv. Phys. **60**, 5 (2011).
[8]M. Farle, Rep. Prog. Phys. **61**, 755 (1998).
[9]M. T. Johnson, P. J. H. Bloemen, F. J. A. Den Broeder, and J. J. de Vries, Rep. Prog. Phys. **59**, 1409 (1996).
[10]P. Poulopoulos, V. Kapaklis, P. E. Jönsson, E. Th. Papaioannou, A. Delimitis, S. D. Pappas, D. Trachylis, and C. Politis, Appl. Phys. Lett. **96**, 202503 (2010).
[11]P. Poulopoulos, S. D. Pappas, V. Kapaklis, P. E. Jönsson, E. Th. Papaioannou, A. Delimitis, D. Trachylis, M. J. Velgakis, E. I. Meletis, and C. Politis, J. Nano Res. **15**, 95 (2011).
[12]G. S. D. Beach, A. E. Berkowitz, F. T. Parker, and D. J. Smith, Appl. Phys. Lett. **79**, 224 (2001).
[13]W. D. Callister, Jr., *Materials Science and Engineering: An Introduction*, 5th ed. (Wiley, New York, 2000).
[14]P. Poulopoulos, M. Angelakeris, E. Th. Papaioannou, N. K. Flevaris, D. Niarchos, M. Nyvlt, V. Prosser, S. Visnovsky, Ch. Mueller, P. Fumagalli, F. Wilhelm, and A. Rogalev, J. Appl. Phys. **94**, 7662 (2003).
[15]H. Kiessig, Ann. Phys. (Leipzig) **402**, 715 (1931).
[16]M. Björck and G. Andersson, J. Appl. Crystallogr. **40**, 1174 (2007).
[17]D. Spiga, Ph.D. dissertstion, University of Milano-Bicocca, 2004–2005.
[18]K. Amemiya and M. Sakamaki, Appl. Phys. Lett. **98**, 012501 (2011).
[19]E. E. Fullerton, J. Pearson, C. H. Sowers, S. D. Bader, X. Z. Wu, and S. K. Sinha, Phys. Rev. B **48**, 17432 (1993).
[20]V. Karoutsos, P. Poulopoulos, V. Kapaklis, S. D. Pappas, D. Trachylis, and C. Politis, J. Nanosci. Nanotechnol. **10**, 6120 (2010) and references therein.
[21]D. P. Pappas, K.-P. Kämper, and H. Hopster, Phys. Rev. Lett. **64**, 3179 (1990).
[22]D. P. Pappas, C. R. Brundle, and H. Hopster, Phys. Rev. B **45**, R8169 (1992).
[23]P. J. Jensen and K. H. Bennemann, Int. J. Mod. Phys. B **7**, 492 (1993).
[24]Ch. Kittel, *Introduction to Solid State Physics*, 5th ed. (Wiley, New York, 1976).
[25]F. Wilhelm, U. Bovensiepen, A. Scherz, P. Poulopoulos, A. Ney, H. Wende, G. Ceballos, and K. Baberschke, J. Magn. Magn. Mater. **222**, 163 (2000).
[26]B. E. Argyle, S. H. Charap, and E. W. Pugh, Phys. Rev. **132**, 2051 (1963).
[27]B. Y. Jin and J. B. Ketterson, Adv. Phys. **38**, 189 (1989).
[28]A. N. Anisimov, W. Platow, P. Poulopoulos, W. Wisny, M. Farle, K. Baberschke, P. Isberg, B. Hjörvarsson, and R. Wäppling, J. Phys.: Condens. Matter **9**, 10581 (1997).
[29]E. Th. Papaioannou, P. Poulopoulos, M. Angelakeris, K. S. Zeimbekis, and N. K. Flevaris, Phys. Status Solidi A **189**, 717 (2002).
[30]H. B. Callen and E. Callen, J. Phys. Chem. Solids **27**, 1271 (1966).
[31]D. P. Pappas, J. Vac. Sci. Technol. B **14**, 3203 (1996).
[32]Kh. Zakeri, Th. Kebe, J. Lindner, and M. Farle, Phys. Rev. B **73**, 052405 (2006).
[33]Kh. Zakeri, Th. Kebe, J. Lindner, and M. Farle, J. Magn. Magn. Mater. **299**, L1 (2006).
[34]O. Fruchart, J.-P. Nozieres, and D. Givord, J. Magn. Magn. Mater. **165**, 508 (1997).
[35]M. Denk, R. Denk, M. Hohage, L. D. Sun, and P. Zeppenfeld, Phys. Rev. B **85**, 014423 (2012).
[36]W. Pan, Y. T. Shih, K. L. Lee, W. H. Shen, C. W. Tsai, D. H. Wei, Y. L. Chan, and H. C. Chang, J. Appl. Phys. **111**, 07C113 (2012).
[37]Z. S. Shan, J. X. Shen, R. D. Kirby, and D. J. Sellmyer, J. Appl. Phys. **75**, 6418 (1994).
[38]S.-K. Kim, V. A. Chernov, J. B. Kortright, and Y. M. Koo, Appl. Phys. Lett. **71**, 66 (1997).
[39]M. J. Hytch, E. Snoeck, and R. Kilaas, Ultramicroscopy **74**, 131 (1998).
[40]M. Ahlberg, G. Andersson, and B. Hjörvarsson, Phys. Rev. B **83**, 224404 (2011).